Carbon 131 (2018) 184–192

Contents lists available at ScienceDirect

Carbon

journal homepage: www.elsevier.com/locate/carbon

Frame-filling C/C composite for high-performance EDLCs with high withstanding voltage

Pan-pan Chang [a, b], Cheng-yang Wang [a, b], Taro Kinumoto [c], Tomoki Tsumura [c], Ming-ming Chen [a, b, c, *], Masahiro Toyoda [c, **]

[a] Key Laboratory for Green Chemical Technology of MOE, School of Chemical Engineering and Technology, Tianjin University, Tianjin 300350, PR China
[b] Collaborative Innovation Center of Chemical Science and Engineering (Tianjin), Tianjin University, Tianjin 300350, PR China
[c] Department of Applied Chemistry, Faculty of Engineering, Oita University, 700 Dannoharu, Oita 870-1192, Japan

ARTICLE INFO

Article history:
Received 6 September 2017
Received in revised form
23 January 2018
Accepted 4 February 2018
Available online 5 February 2018

ABSTRACT

Based on the equation of $E = 1/2CV^2$, increasing voltage can significantly enhance the energy density of electric double-layer capacitors (EDLCs). However, with the voltage above 2.7 V, the lifespan of EDLCs drops rapidly due to the undesired parasitic processes. To operate at voltage above 2.7 V, a frame-filling C/C composite is prepared by constructing relatively perfect carbon network and reducing the oxygen-containing groups. The as-prepared sample F310-800 exhibits high specific surface area (2626 $m^2 g^{-1}$), adequate *e*-conductivity (142 S m^{-1}), high sp^2-bonding carbon content (92.6%) and low oxygen content (4.6 *wt*%). Although totally free of any carbon black, it demonstrates excellent EDLC performances. It can successfully operate at voltage of 3 V in $TEABF_4$/PC electrolyte and obtain high gravimetric capacitance (C_g) of 140 F g^{-1} and volumetric capacitance (C_v) of 57.4 F cm^{-3} at 50 mA g^{-1} with rate capacity $C_{10/0.05}$ as high as 66%. Additionally, at voltage of 3.5 V in pure $EMIMBF_4$ electrolyte, it achieves ultrahigh C_g of 156 F g^{-1} and C_v of 64 F cm^{-3} at 50 mA g^{-1}. Its energy density can reach up to 66.3 Wh kg^{-1}. Meantime, after 5000 cycles at 2.5 A g^{-1}, it holds 91.9% of its initial capacitance.

1. Introduction

As environmental-friendly electrical energy storage devices, electric double-layer capacitors (EDLCs) have a wide range of applications such as portable electronic devices and hybrid electric vehicles [1–4]. They endow high power capability, good lifespan and low maintenance [5–7]. However, the energy density of EDLCs is still lower than that of lithium ion batteries. Therefore, it is of vital importance to increase the energy density of EDLCs without sacrificing their power density and lifespan [8].

Electrode materials are critical in determining the properties of EDLCs and the most commonly used electrode materials for EDLCs are porous carbons [9]. Nowadays, researchers have made a lot of efforts in the design of novel materials to increase the energy density by improving the capacitance of EDLCs, such as porous graphene [10–12], 2D/3D hierarchical porous carbons [13–17] and so on [18]. According to the equation $E = 1/2CV^2$, the energy density has linear square relationship with the voltage. Therefore, increasing voltage is more effective. The maximum voltage of EDLCs in the common tetraethylammonium tetrafluoroborate/propylene carbonate ($TEABF_4$/PC) electrolyte is often limited to 2.5–2.7 V [19]. With the further increase of voltage above 2.7 V, the capacitance and the lifespan will both diminish rapidly. It is because that undesired parasitic processes can occur on the positive and negative electrode of EDLCs, respectively [20–22]. Specifically, on the positive electrode, the oxygen-containing groups on the surface of porous carbons will decompose and generate gaseous products such as CO_2, CO and H_2 [20]. While on the negative electrode, PC solvent will be reduced to form propylene, H_2, CO_2 and CO [20]. These undesired reactions will happen more easily on the defects of porous carbons (such as edge carbon atoms, sp^3-bonding carbon, dangling bonds and so on) [23]. While in pure 1-ethyl-3-methylimidazolium tetrafluoroborate ($EMIMBF_4$) ionic liquid electrolyte with a wide voltage widow of 3.5 V, the capacitance fading under

* Corresponding author. Key Laboratory for Green Chemical Technology of MOE, School of Chemical Engineering and Technology, Tianjin University, Tianjin 300350, PR China.
** Corresponding author. Department of Applied Chemistry, Faculty of Engineering, Oita University, Oita 870-1192, Japan.
E-mail addresses: chmm@tju.edu.cn (M.-m. Chen), toyoda22@oita-u.ac.jp (M. Toyoda).

https://doi.org/10.1016/j.carbon.2018.02.022
0008-6223/

long-time cycle tests can be influenced by the autocatalytic effects of sp^2-bonding carbon on the decomposition of electrolytes under applied voltage, proved by Romann's group using spectro-electrochemistry method [24,25]. On the positive electrode, catalyzed by the sp^2-bonding carbon surface, the electrochemical fluorination of ionic liquid can occur to form the imidazolium trifluoroborate derivants. While on the negative electrode, the imidazolium cations can decompose to form the dimer and H_2.

Pursuing higher voltage, many researches have focused on constructing perfect carbon networks by controlling the surface defect. Hata's group constructed single walled carbon nanotube (SWCNT)-based EDLC electrode with high carbon purity of 99.98% and negligible carbonaceous impurity (less than 2% amorphous carbon). It can operate at ultrahigh voltage of 4 V in $TEABF_4$/PC electrolyte [26]. Yang's group synthesized a partially graphitized porous carbon which can operate at the voltage of 3 V in $TEABF_4$/PC electrolyte [27]. Ruoff's group obtained porous graphene sheets with 98% sp^2-bonding carbon and low content of edge carbon atoms. In 1-butyl-3-methyl-imidazolium tetrafluoroborate/acetonitrile ($BMIMBF_4$/AN) electrolyte, the voltage can reach up to 3.5 V [28]. Another effective approach to increase the operation voltage is to reduce the oxygen-containing group content. Gao's group reported that vacuum annealing can largely reduce the oxygen-containing groups on the porous carbon surface. And the vacuum annealing-treated porous carbon can operate at voltage of 3.5 V in 1-ethyl-3-methyl-imidazolium bis(tri-fuoromethylsulfonyl)imide (EMIMTFSI), showing high energy density and good cycle stability [29]. Shiraishi's group also observed that the thermal treatment under H_2 atmosphere can effectively decrease the oxygen-containing groups and purify the surface of porous carbon, which enable a much lower degradation of the EDLC electrode even at the voltage of 3 V in $TEABF_4$/PC electrolyte [30]. Therefore, all these studies have demonstrated that only if the porous carbon owns (1) perfect carbon network structure (high sp^2-bonding carbon content) and (2) low content oxygen-containing groups, it can operate at higher working voltage.

Fortunately, in previous work, we have constructed a frame-filling nanoporous C/C composite, which had relatively perfect carbon networks with high sp^2-bonding carbon content [31,32]. Furthermore, in this paper, we discovered that after high temperature annealing, the C/C composite had not only relatively perfect carbon networks but also low content oxygen-containing groups. When used as EDLC electrode, it can successfully operate at the/a voltage of 3 V in $TEABF_4$/PC electrolyte and at the/a voltage of 3.5 V in pure $EMIMBF_4$ electrolyte with high energy density, high power density and good lifespan.

2. Experimental

2.1. Synthesis of the C/C composites

Graphite oxide and CP-A5 were respectively synthesized from natural flake graphite and coal tar pitch with a softening point of 85 °C, described in previous work [31–35].

A frame-filling C/C composite was prepared from a mixture of CP-A5 and graphite oxide by KOH activation, with some modifications to *F*-case method described in previous publication [31,32]. The only difference is that after activation, the sample was further treated by annealing up to 800 °C at a rate of 2 °C min^{-1} under N_2 atmosphere without any holding, named F310-800. The sample without annealing was a reference, named F310. As for the name, F310-800 represents the sample synthesized by method *F* and annealing at 800 °C. The first Arabic number 3 means the mass ratio of KOH to the total carbon precursors; the second and third Arabic number 10 together represent the percentage of graphite oxide content; the last Arabic number 800 means that the annealing temperature is 800 °C.

2.2. Structural characterization

Powder X-ray diffraction (XRD) patterns were analyzed on a Rigaku D/Max 2500 v/PC system using Cu Kα radiation (40 kV, 200 mA, $\lambda = 1.54051$ Å). Raman spectra were conducted on a Renishaw MKI-2000 Raman microscope at 532 nm. X-ray photoelectron spectroscopy (XPS) measurement was obtained on a PHI-1600 ESCA electron system (America PE Company) using Al Kα (1486.6 eV) radiation. The atom percentages of C, N, S and O can be determined by the regular scanning analysis. Elemental measurement was conducted with a Vario EL III elemental analyzer (Elementar, Germany). The weight percentages of C, H, N, S and O can be determined by direct analysis. The surface morphologies were analyzed on Philips XL30 (FESEM, Nano 430) scanning electron microscopy (SEM) and Philips Tecnai G2 F20 transmission electron microscopy (TEM). Porous structures were characterized by N_2 adsorption/desorption at 77 K (Micrometrics ASAP 2020). The specific surface area (SSA) and pore size distributions were obtained by the Brunauer-Emmett-Teller (BET) method and nonlocal density function theory (NLDFT) method, respectively. The bulk *e*-conductivity of samples was analyzed on RTS-9 type four-point probe instrument. Electron energy loss spectroscopy (EELS) was also conducted on the Philips Tecnai G2 F20 TEM by STEM mode (Fig. S5).

2.3. Electrochemical measurements

All the electrodes were of 1.3 cm in diameter and 200 μm in thickness. To meet the requirement of commercial standard EDLCs, the electrode thickness of 200 μm is very close to the industry-level. The electrodes were fabricated by mixing 90% active material with 10% poly (tetrafluoroethylene) (PTFE, 65 wt% dispersion in water) together. The areal mass loading of active materials in a single electrode was 7.8–8.2 mg cm^{-2}. And the active material densities (ρ) of F310 electrode and F310-800 electrode were determined as 0.392 g cm^{-3} and 0.41 g cm^{-3}, respectively. The conductive carbon coated aluminum foil (30 μm) and cellulose paper were respectively used as current collector and separator. The electrolytes were 1 M $TEABF_4$/PC and pure $EMIMBF_4$. For the cell assembly, a pair of typical electrodes with equal mass was assembled in a glove box filled with Ar after drying overnight at 120 °C under vacuum. All the electrochemical performances were measured in two-electrode symmetric supercapacitor. Cyclic voltammetry (CV) and electrochemical impedance spectroscopy (EIS) tests were conducted on Princeton PARSTAT 2273 electrochemical workstation. Nyquist plots were recorded at frequencies from 100 kHz to 10 mHz at room temperature. For CV tests, the voltage sweep rates were from 20 mV s^{-1} to 100 mV s^{-1} in both electrolytes. Galvanostatic charge/discharge (GCD) tests were performed on Arbin battery test system at current densities from 0.05 to 10 A g^{-1} in both electrolytes. The potential ranges were 0–2.7 V and 0–3 V in 1 M $TEABF_4$/PC electrolyte, while the potential range was 0–3.5 V in neat $EMIMBF_4$ electrolyte. The gravimetric specific capacitance (C_g), the volumetric specific capacitance (C_v), the gravimetric energy density (E_g), the average gravimetric power density (P_g), the volumetric energy density (E_v), the average volumetric power density (P_v) were calculated by Ref. [36]:

$$dV/dt = (V_{max}\text{-}V_{1/2max})/(t_{1/2max}\text{-}t_{max}) \quad (1)$$

$$C = I/(dV/dt) \quad (2)$$

$$C_g = 4C/m \quad (3)$$

$$C_v = \rho^* C_g \quad (4)$$

$$E_g = 1/8^* C_g{}^* V^2 \quad (5)$$

$$P_g = 3600^* E_g/t_{max} \quad (6)$$

$$E_v = 1/8^* C_v{}^* V^2 \quad (7)$$

$$P_v = 3600^* E_v/t_{max} \quad (8)$$

where C stands for the capacitance (F) of total capacitor and C_g stands for the gravimetric specific capacitance (F g^{-1}) for the active material in a single electrode, I is the current (A), m is the total mass of active materials (g) in a device, V_{max} and t_{max} represent the maximum discharge voltage (V) and corresponding time (s), $V_{1/2max}$ and $t_{1/2max}$ represent the half of maximum discharge voltage (V) and corresponding time (s), V represents the operating voltage (V, obtained from the discharge curve by subtracting V_{drop} from V_{max}), C_v stands for the volumetric specific capacitance (F cm^{-3}) for the active material in a single electrode, E_g and P_g are respectively the gravimetric energy density (Wh kg^{-1}) and average gravimetric power density (W kg^{-1}) of the total capacitor, E_v and P_v are respectively the volumetric energy density (Wh L^{-1}) and average volumetric power density (W L^{-1}) of the total capacitor.

3. Result and discussion

3.1. Surface morphology and effect of sp^2-bonding carbon content on the conductivity of porous carbon

TEM images (Fig. 1) show that sample F310-800 is typical C/C composite with integrative carbon networks, without morphology difference from un-annealed sample F310 [32]. It is of frame-filling structure, in which the frame is composed of graphene oxide-derived carbon while the filling parts come from CP-A5-derived porous spheres with size of 20–50 nm. Both graphene oxide and CP-A5 are hydrophilic, facilitating an easy self-organization in alkali liquid. Fortunately, alkali environment additionally catalyzes the nucleophilic addition between some certain surface groups belonging to graphene oxide or CP-A5. Thus this kind of self-organization is based on chemical bonding, C-O-C bond in specific [31]. From the HR-TEM images in Fig. 1b&c (the edge of C/C composite), the graphene microsheet moieties have lamellar graphitic structures and slight pores. Totally different, the nano-sized carbon moieties have turbostratic graphitic structure and abundant pores. Notably, such integrative structure is deemed to well-balance the relationship between developed pore structure and *e*-conductivity. On the one hand, nano-sized carbon particles can furnish many adsorption sites for the electrolyte ion storage. On the other hand, the few-layer graphene microsheets can serve as conductive network to insure high *e*-conductivity.

The *e*-conductivity of porous carbon is highly relevant to the sp^2-bonding carbon content, which can be calculated from EELS by measuring the peak area ratio of π^* bonding to $\pi^*+\sigma^*$ bonding and XPS (Fig. 3) by measuring the peak area ratio between sp^2 carbon and the sum of sp^2 carbon and sp^3 carbon [28,37]. As shown in Fig. 1d, π^* bonding (energy loss range from 282.5 to 287.5 eV) represents the sp^2-bonding carbon, while σ^* bonding (energy loss range from 287.5 to 310.5 eV) represents the sp^3-bonding carbon. Assuming that reference graphite has 100% sp^2-bonding carbon content, sample F310-800 with annealing has higher sp^2-bonding carbon content of 92.6% than that of F310 without annealing (88.2%). Hence, the *e*-conductivity increases by 18.3% from 120 S m^{-1} of F310 to 142 S m^{-1} of F310-800 (Table 1). The higher *e*-conductivity illustrates that F310-800 has more ideal graphitic crystals than F310 (proved by XRD and Raman results). It is because that high temperature annealing can reorganize the carbon skeleton, decrease the mechanical stress of carbon material and thus form more stable structures [29]. The above results reveal that F310-800 owns perfect carbon networks, which is pivotal for EDLCs operating at high withstanding voltage. In addition, because the high *e*-conductivity of 142 S m^{-1} is enough to guarantee good

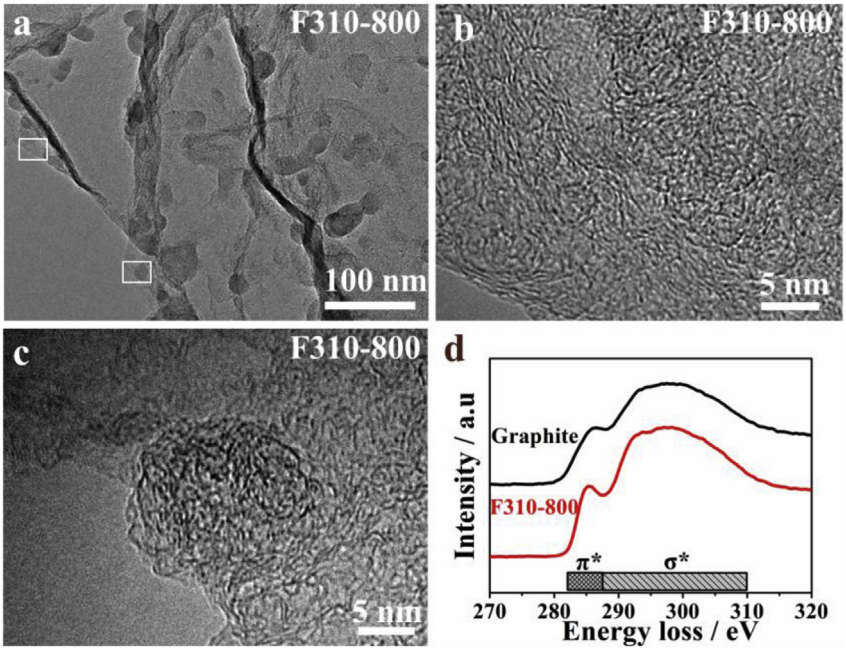

Fig. 1. TEM image (a) of F310-800; HR-TEM images (b, c) of the edge of F310-800 (enlarged from the white rectangular box in Fig. 1a); EELS (d) of F310-800 and graphite (as a reference). (A colour version of this figure can be viewed online.)

Table 1
The *e*-conductivity and sp^2-bonding carbon content of F310 and F310-800 by EELS and XPS.

Sample	*e*-conductivity[a] (S/m)	$\frac{sp^2}{sp^2+sp^3}$*100%	
		From EELS	From XPS
F1310 [32]	120	88.2	86.3
F310-800	142	92.6	91

[a] The electrical conductivity was tested by four-point probe method.

electrical contact, F310-800 can be used as conductive agent-free EDLC electrode.

3.2. Physical structure of porous carbon

XRD spectra of F310 and F310-800 are displayed in Fig. 2a. Two weak and broad peaks at around 24° and 43° are assigned to (002) and (100) peaks of amorphous carbon layers, respectively. It suggests that there exist no long-range ordered structures in both samples [5]. The remarkable intensities in the low-angle scatter represent the presence of many micropores. In comparison to F310 without annealing [32], the (002) peak of F310-800 with annealing shifts to higher angle of 25.02° with smaller interlayer space d_{002} of 0.3556 nm (Table 2). Furthermore, F310-800 has smaller crystal size L_c (0.75 nm) and planar aromatic size L_a (4.38 nm) than F310 (Table 2). The amorphous structures of F310 and F310-800 are also proved by Raman spectra in Fig. 2b. The peaks at around 1350 and 1590 cm^{-1} are attributed to the D band (defects) and G band (graphite) of carbon materials. Generally, the D band corresponds to the disordered carbons and the G band represents the ordered graphitic carbons [38]. The I_D/I_G ratio can be used to calculate the graphitization degree of the carbon material. After high temperature annealing, the I_D/I_G value decreases from 1.924 of F310 to 1.74 of F310-800 (Fig. 2b), implying higher graphitization degree in F310-800 (consistent with EELS and XRD observations). It suggests that the thermal treatment can rearrange the carbon skeleton and reduce the defects to some extent, thus improving the graphitic microcrystallines of porous carbons.

3.3. XPS and elemental analysis of porous carbons

C 1s and O 1s spectra of porous carbons (Fig. 3) clearly reveal the effect of high temperature annealing on the content and chemical state of carbon atoms and oxygen atoms. In both samples (Fig. 3a&c), the dominant C 1s peak at 284.6 eV and weak C 1s peak at 285.3 eV are respectively assigned to sp^2-bonding carbon and sp^3-bonding carbon. Besides, three weaker peaks at higher binding energy correspond to C-O peak at 286.4 eV, C=O peak at 288 eV and COOH or π-π^* at 289 eV [39,40]. After high temperature annealing, the peak intensities representing the oxygen-containing groups in F310-800 decrease obviously (Fig. S6). This is also proved by O 1s spectra (Fig. 3b&d). Three peaks at 531.1 eV, 532.3 eV and 533.7 eV are respectively attributed to C=O peak in carbonyl or quinone, C-O peak in ether or phenol, and COOH [29]. It can be clearly seen that (1) the total contents of oxygen-containing groups in F310-800 decrease visibly compared with F310; (2) the contents of C-O group and C=O group in F310-800 increase up to 89.9%, higher than F310 of 76.2% (Fig. 3b&d). It has been reported that as for EDLCs in $TEABF_4$/PC electrolyte upon over-voltage (above 2.7 V), the COOH group is most unstable which can decompose at voltage of 3.0 V; while the C-O group (ether or phenol) and C=O group (carbonyl or quinone) are relatively more stable which can decompose at voltage above 3.3 V [20–22]. Therefore, F310-800-based EDLC is much more stable than F310-based EDLC when operating at voltage of 3 V in $TEABF_4$/PC electrolyte.

F310-800 has much lower O content both in bulk and on its surface than F310 (Table 3). It elucidates that high temperature annealing can eliminate the oxygen-containing groups to a certain degree, not only on the surface but also inside the carbon materials.

3.4. Pore structure of porous carbon

The N_2 adsorption/desorption isotherm of F310-800 is of particular type IV with hysteresis loops, implying high mesopore content (Fig. 4a), proved by the pore size distribution in Fig. 4b. F310-800 possesses typical hierarchical pore structure, namely, prevailing micropores, moderate mesopores and slight macropores. The micropore size mainly locates around 0.54 nm, 0.79 nm, 1.17 nm and 1.59 nm, which plays critical role in the storage of electrolyte ions. The mesopores with wide pore size range are beneficial for fast electrolyte ion transmission. And the macropores act as ion-buffering reservoir. The pore structure parameters of F310-800 and the reference sample F310 are presented in Table 4. The SSA of F310-800 is 2626 $m^2 g^{-1}$ with 39% mesopore content, with small difference with that of F310. However the pore volume decreases obviously. The micropore volume changes a little, whereas the mesopore volume decreases by 32% from 1.78 $cm^3 g^{-1}$ of F310 to 1.21 $cm^3 g^{-1}$ of F310-800. It illustrates that high temperature annealing can mainly cause the shrinkage of mesopores and thus diminish the mesopore volume. The high SSA and hierarchical pore structure endow F310-800 competitive as EDLC electrode material.

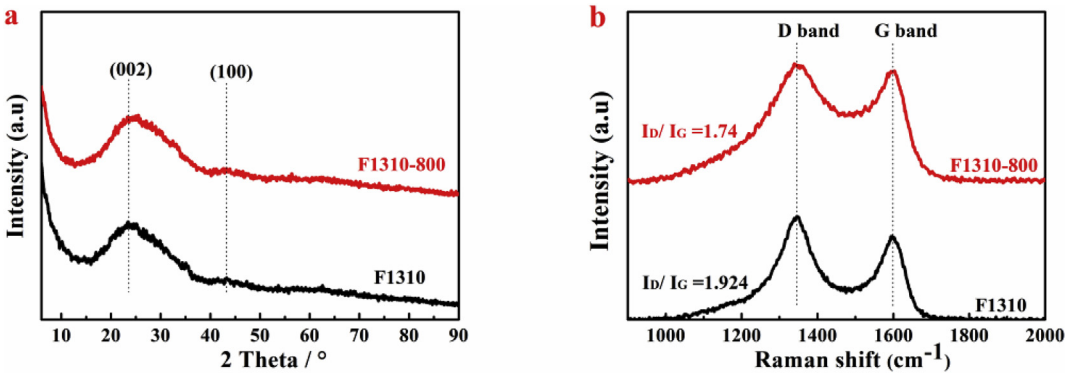

Fig. 2. XRD (a) and Raman spectra (b) of F310 and F310-800 (I_D/I_G was calculated by the integral peak area ratio of D band and G band). (A colour version of this figure can be viewed online.)

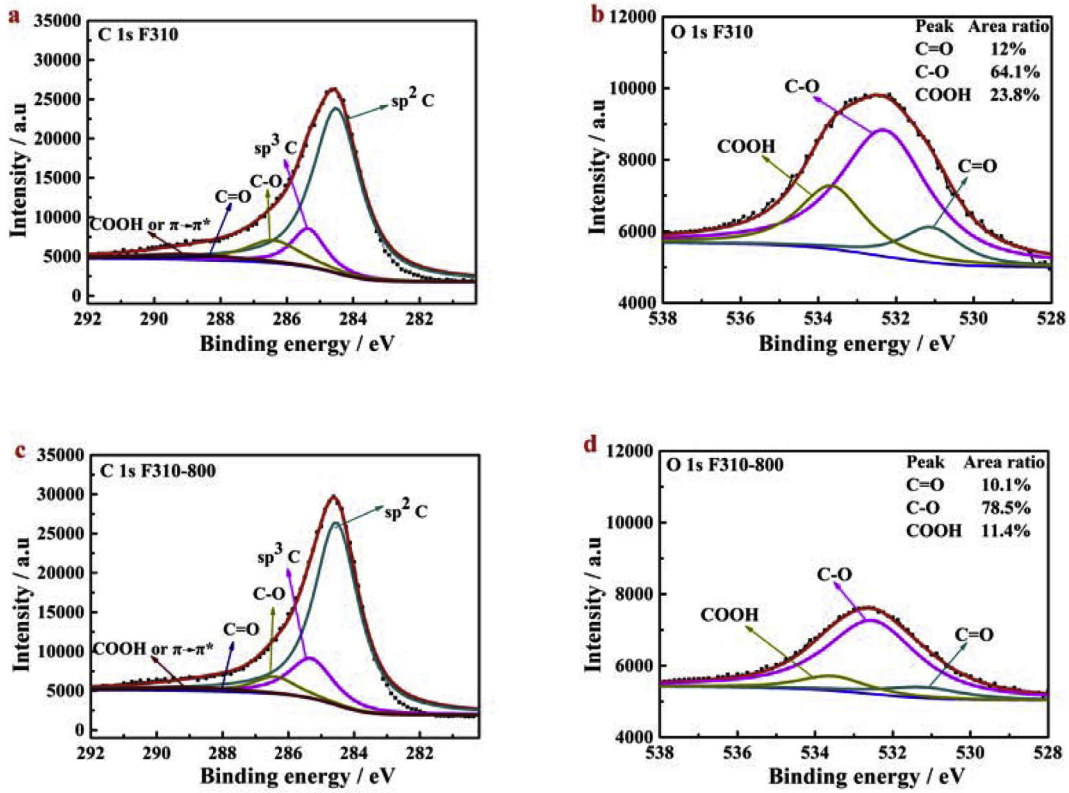

Fig. 3. C 1s (a, c) and O 1s (b, d) XPS spectra of F310 and F310-800. (A colour version of this figure can be viewed online.)

Table 2
XRD parameters of F310 and F310-800.

Sample	$2\theta_{002}$/°	d_{002}/nm	L_c/nm	$2\theta_{100}$/°	L_a/nm
F310 [32]	23.42	0.3795	0.93	43.28	4.93
F310-800	25.02	0.3556	0.75	43.7	4.38

Table 3
Surface atom analysis by XPS and elemental analysis of bulk porous carbons.

Sample	Elemental analysis (*wt*/%)					Surface atom analysis (*at*/%)				
	C	N	H	S	O	C	N	S	O	C/O
F310	85.2	1.25	0.71	1	11.84	89.3	0.6	0.4	9.7	9.2
F310-800	93.1	1.1	0.6	0.6	4.6	95.3	0.3	0.2	4.2	22.7

3.5. Electrochemical properties of porous carbons

In our previous work, the frame-filling C/C composite showed excellent properties as EDLC electrode. However, its energy density was still lower than that of most reported electrode materials. Based on the above results, F310-800 with annealing owns relatively perfect carbon network and low content oxygen-containing groups. These two factors are of vital importance for EDLCs operating at high voltage. For application aspect, it is necessary to investigate the effect of different operating voltage on the electrochemical performances of porous carbons.

Nyquist plots (Fig. 5a and Fig. S8) provide reliable information on the dynamic diffusion of electrolyte ion into electrode. The equivalent series resistance (R_S) (the first point in the high

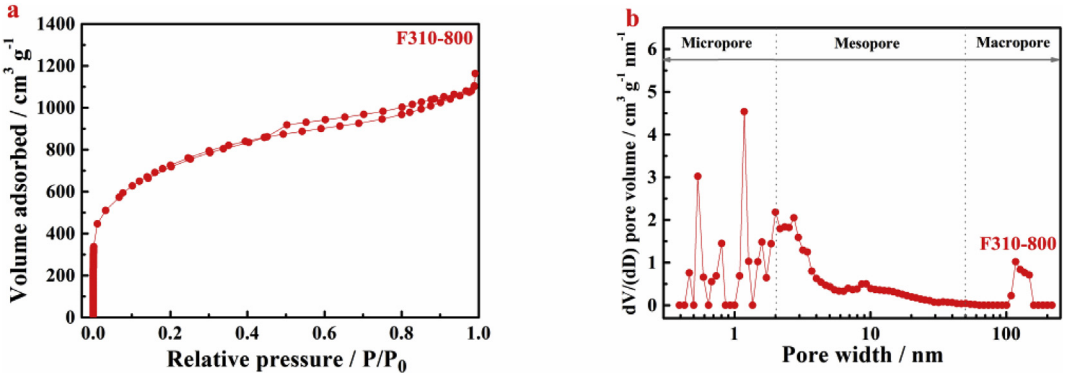

Fig. 4. Type IV N_2 adsorption/desorption isotherm (a) and pore size distribution calculated by NLDFT model (b) of F310-800. (A colour version of this figure can be viewed online.)

Table 4
Pore structure parameters of F310 and F310-800.

Sample	S_{BET} ($m^2\ g^{-1}$)	S_{mes} ($m^2\ g^{-1}$)	S_{mic}[a] ($m^2\ g^{-1}$)	V_{tot} ($cm^3\ g^{-1}$)	V_{mes} ($cm^3\ g^{-1}$)	V_{mic}[a] ($cm^3\ g^{-1}$)	S_{mes}/S_{BET} (%)
F310 [32]	2562	979	1583	2.34	1.78	0.56	38.2
F310-800	2626	1024	1602	1.8	1.21	0.59	39

[a] $S_{mic} = S_{BET} - S_{mes}$; $V_{mic} = V_{tot} - V_{mes}$.

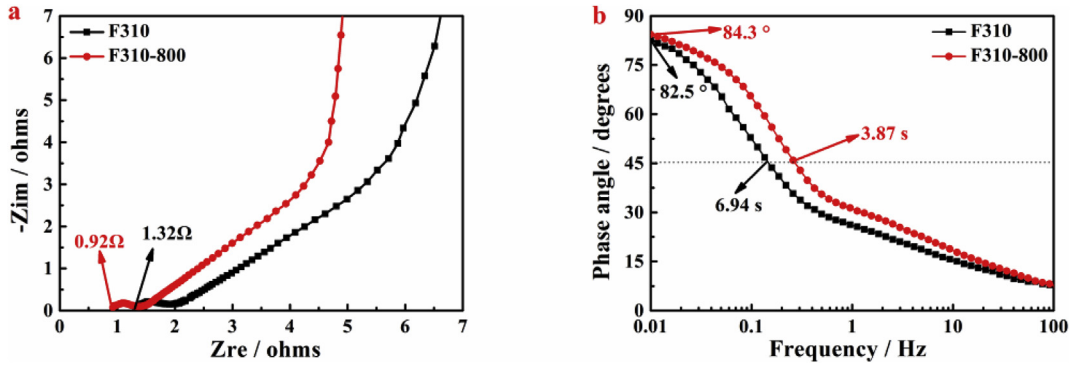

Fig. 5. Nyquist plots (a) and the impedance phase angle *vs* frequency (b) of F310 and F310-800 electrode in 1 M $TEABF_4$/PC electrolyte. (A colour version of this figure can be viewed online.)

frequency region) is highly relevant to the overall internal resistance of electrode. Due to higher *e*-conductivity, the R_S of F310-800 is only 0.92 Ω in 1 M $TEABF_4$/PC electrolyte, much smaller than that of F310 (Fig. 5a). Meanwhile F310-800 has smaller Warburg resistance than F310 (Table S4). It illustrates that F310-800 has more unimpeded pathways for the speedy ion transport into the pores (consistent with the results of N_2 adsorption/desorption curves in Fig. 4). The impedance phase angle *vs* frequency is shown in Fig. 5b. At low frequency of 0.01 Hz, the phase angles of F310−800 and F310 are respectively 84.3° and 82.5°. It suggests that compared with F310-based EDLC, F310-800-based EDLC is closer to an ideal capacitor. The frequency at a phase angle of 45° means the point where the resistive and capacitive impedances are equal. The corresponding relaxation time constant ($\tau_0 = 1/f$) represents how fast the EDLC device can run reversibly. The τ_0 is only 3.87 s for F310-800, 44% faster than F310 (6.94 s), making F310-800 competitive for multiple serial-parallel EDLC devices.

The comparison GCD and CV curves of F310 and F310-800 (Fig. 6a&b) are evaluated in $TEABF_4$/PC electrolyte within voltage from 0 to 2.7 V and from 0 to 3 V. As for F310-800 with annealing, the GCD curve from 0 to 3 V coincides exactly with that from 0 to 2.7 V, implying little capacitive dependence on voltage. While slight voltage dependence is discovered for F310 without annealing. Its GCD curve from 0 to 3 V has slight difference with that from 0 to 2.7 V, proved by CV test in Fig. 6b. As for F310-800, the CV curve from 0 to 3 V overlaps with that from 0 to 2.7 V. But for F310, the CV curve from 0 to 3 V shows a loss of electrochemical active area compared with that from 0 to 2.7 V. The results indicate that F310-800 with annealing can commendably operate at voltage of 3 V. The rate performances of F310 and F310-800 at different operation voltage are shown in Fig. 6c. At 3 V and 50 mA g^{-1}, F310 gets C_g of 128 F g^{-1} with rate capacity $C_{10/0.05}$ of only 50%. Surprisingly, F310-800 gets 140 F g^{-1} and better $C_{10/0.05}$ of 66% (92.1 F g^{-1} at 10 A g^{-1}). Based on the electrode densities (ρ) of F310 (0.392 g cm^{-3}) and F310-800 (0.41 g cm^{-3}), the C_V of F310 and F310-800 are calculated to be 41.9 and 54.1 F cm^{-3} at 1 A g^{-1}, respectively (Fig. 6c and Table S6). Although the impact of operating voltage on rate performance is slight, its influence on lifespan of the EDLCs is demonstrated to be great (Fig. 6d). At 2.7 V, the capacitance retentions of F310−800 and F310 electrode after 10,000 cycles are respectively 92.1% and 80.2%, with only 11.9% difference. However, at a higher working voltage of 3 V, the difference becomes more pronounced. F310-800 still retains 82.1% of its initial capacitance, while F310 only lefts 59.9% of its initial capacitance. The poor capacitance retention of F310 is caused by its high content of oxygen-containing groups (Table 3), which could decompose at voltage of 3 V and thus decay the electrode. It is noteworthy that the favorite lifespan of F310-800 results from its relatively perfect carbon network and low content oxygen-containing groups.

Energy density of F310-800 can be much improved because it withstands applying voltage even up to 3.5 V in pure ionic liquid $EMIMBF_4$ electrolyte. The symmetric triangular GCD curves in Fig. 7a illustrate the ideal capacitor behaviors of F310-800. The C_g of F310-800 is as high as 156 F g^{-1} (C_V of 64 F cm^{-3}) at 50 mA g^{-1} and 61% of the C_g value (95 F g^{-1}) is retained at 10 A g^{-1} (Fig. 7c). The CV curves of F310-800 (Fig. 7b) exhibit apparent turnup tails within voltage from 3 to 3.5 V, implying the polarization phenomenon. After 5000 cycles at 2.5 A g^{-1}, F310-800 could still retain 91.9% of its initial capacitance (Fig. 7d), showing its excellent cycling stability owing to stable carbon surfaces and structural network. And the electrochemical fluorination of $EMIMBF_4$ on the positive electrode is the main reason for the lifetime decay of F310-800-based EDLC [24,25], proved by the CV curves (Fig. 7b). Interestingly, the electrochemical performances of F310-800 in $EMIMBF_4$ are notably superior to those in $TEABF_4$/PC. It is because that the pore size distribution of F310-800 is more suitable for $EMIMBF_4$ electrolyte (Fig. 4b). The pore size of 0.54 nm can be exactly applicable for $EMIM^+$ ion (0.43 nm), but not for TEA^+ ion (0.68 nm), which thus can largely improve the electrochemical performances in $EMIMBF_4$ electrolyte [29].

Ragone plot (Fig. 8 and Fig. S11) further illustrates the overall energy and power output of EDLCs. In $TEABF_4$/PC electrolyte, at voltage of 2.7 and 3 V, F310-800 owns higher output characteristics in terms of both energy density and power density. With the voltage increasing from 2.7 to 3 V, the energy density increases 23.4% from 35.4 Wh kg^{-1} (14.5 Wh L^{-1}) to 43.7 Wh kg^{-1} (17.9 Wh L^{-1}). F310-800 performs even better in pure $EMIMBF_4$. Its energy density increases up to 66.3 Wh kg^{-1} (27.2 Wh L^{-1}) at power

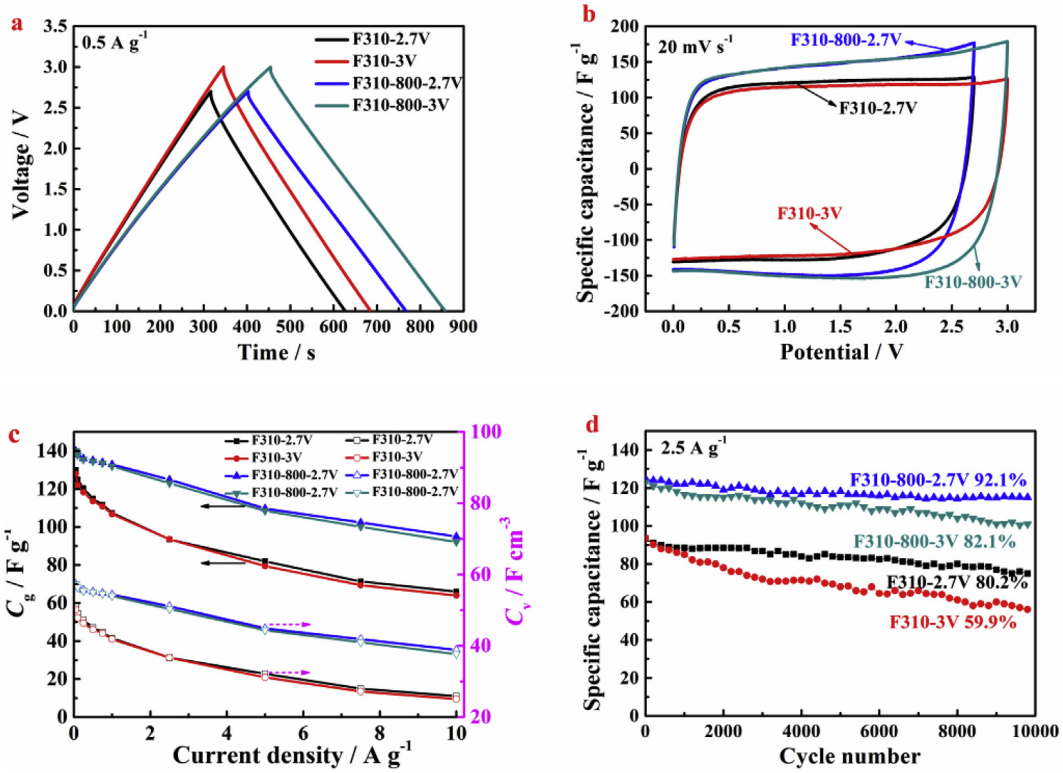

Fig. 6. GCD curves at 0.5 A g^{-1} (a) and CV curves at 20 mV s^{-1} (b) of F310 and F310-800 in 1 M $TEABF_4$/PC electrolyte; rate performances (c) and life spans (d) of F310 and F310-800 at 2.5 A g^{-1} in 1 M $TEABF_4$/PC electrolyte. All tests were in two-electrode systems. (A colour version of this figure can be viewed online.)

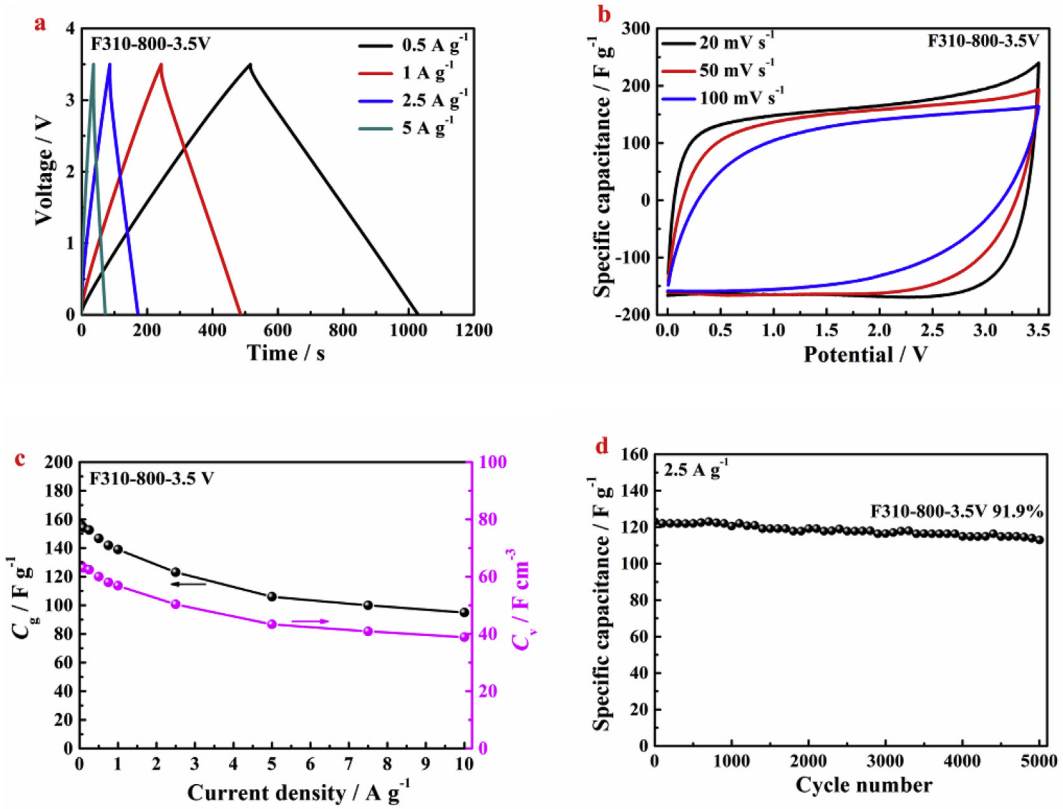

Fig. 7. GCD curves at different current density (a); CV curves at different scan rate (b); rate performances (c) and life span at 2.5 A g^{-1} (d) of F310-800 in pure $EMIMBF_4$ electrolyte. All tests were in two-electrode systems. (A colour version of this figure can be viewed online.)

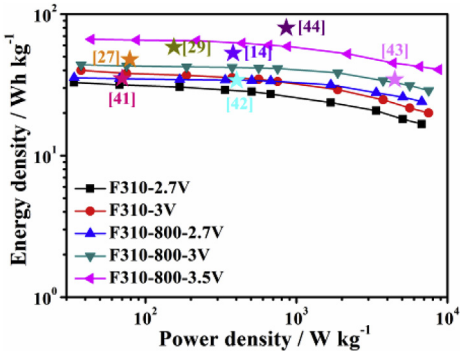

Fig. 8. Ragone plots of F310 and F310-800 in 1 M $TEABF_4$/PC or pure $EMIMBF_4$ electrolyte, *vs.* CK-850@$TEABF_4$/PC-2.7 V [41], PGPC@$TEABF_4$/PC-3 V [27], [rGO-CNT]@$TEABF_4$/PC-3 V [42], IMPC@$LiPF_6$/EC-DMC-3 V [43], PCNS-6@$EMIMBF_4$-3 V [14], BHNC@EMIMTFSI-3.5 V [29] and GPC@EMIMTFSI-3.5 V [44] (based on the gravimetric energy density and the average gravimetric power density). (A colour version of this figure can be viewed online.)

density of 43.7 W kg^{-1} (17.9 W L^{-1}) and still retains 40.5 Wh kg^{-1} (16.6 Wh L^{-1}) at higher power density of 8750 W kg^{-1} (3587 W L^{-1}). These values are comparable to some porous carbons in literature, shown in Fig. 8 [14,27,29,41–44]. Assuming the content of F310-800 in a commercial EDLC device was of 30%, F310-800-based device (in $EMIMBF_4$ electrolyte) would own energy density of 19.9 Wh kg^{-1} (8.16 Wh L^{-1}) based on rough estimation. It is superior to the performance of present commercial AC-based devices (5 Wh kg^{-1}, in general) [28,45–47].

In sum, F310-800 can successfully operate at voltage of 3 V in $TEABF_4$/PC electrolyte and at voltage of 3.5 V in $EMIMBF_4$ electrolyte. Its high SSA, hierarchical pore structure and adequate *e*-conductivity are beneficial for the high specific capacitance and excellent rate capacity. More importantly, its perfect carbon network and low content oxygen-containing groups guarantee the long lifespan at high operation voltage window. These factors together endow synergistic energy and power output characteristic of F310-800-based EDLC. The excellent gravimetric EDLC performances of F310-800 are comparable to and even precede previously reported EDLC electrode materials with high withstanding voltage, including pure graphene or CNT-based porous carbons [42,48,49], 2D/3D architecture-based porous carbons [14,27,29,41,43,44] shown in Table S5. However, due to the low electrode density (0.41 g cm^{-3}) of F310-800, the volumetric performance of F310-800 is still lower than that of reported EDLC electrode materials (Table S6). In this regard, greater efforts should be made in our future research.

4. Conclusions

In this paper, a frame-filling C/C composite was synthesized from a mixture of coal tar pitch-based carbonaceous material and graphite oxide by simple KOH activation and high temperature annealing. It owns high SSA, hierarchical pore structure and adequate *e*-conductivity. Moreover, it possesses relatively perfect carbon network and low content oxygen-containing groups, which are of vital importance for EDLCs operating at high voltage. Different from the reported EDLC electrode materials whose operation voltage is often limited to 2.5–2.7 V, this C/C composite can successfully operate at voltage of 3 V in $TEABF_4$/PC electrolyte and at voltage of 3.5 V in pure $EMIMBF_4$ electrolyte. In both electrolytes, it can acquire high gravimetric specific capacitance, excellent rate capacity and outstanding lifespan. The excellent EDLC performances at high operation voltage benefit from the relatively perfect carbon network and low content oxygen-containing groups, which make the undesired parasitic processes very limited.

Acknowledgments

This work was supported by the National Natural Science Foundation of China (NSFC 51372168) and the Natural Science Foundation of Tianjin City (Key program, 17JCZDJC36800).

Appendix A. Supplementary data

Supplementary data related to this article can be found at https://doi.org/10.1016/j.carbon.2018.02.022.

References

[1] Z. Liu, K. Xiao, H. Guo, X. Ning, A. Hu, Q. Tang, et al., Nitrogen-doped worm-like graphitized hierarchical porous carbon designed for enhancing area-normalized capacitance of electrical double layer supercapacitors, Carbon 117 (2017) 163–173.
[2] B. Li, F. Dai, Q. Xiao, L. Yang, J. Shen, C. Zhang, et al., Nitrogen-doped activated carbon for a high energy hybrid supercapacitor, Energy Environ. Sci. 9 (1) (2016) 102–106.
[3] H. Itoi, H. Nishihara, T. Kyotani, Effect of heteroatoms in ordered microporous carbons on their electrochemical capacitance, Langmuir 32 (46) (2016) 11997–12004.
[4] F. Cao, M. Zhao, Y. Yu, B. Chen, Y. Huang, J. Yang, et al., Synthesis of two-dimensional CoS1. 097/nitrogen-doped carbon nanocomposites using metal–organic framework nanosheets as precursors for supercapacitor application, J. Am. Chem. Soc. 138 (22) (2016) 6924–6927.
[5] H. Feng, M. Zheng, H. Dong, Y. Xiao, H. Hu, Z. Sun, et al., Three-dimensional honeycomb-like hierarchically structured carbon for high-performance supercapacitors derived from high-ash-content sewage sludge, J. Mater. Chem. 3 (29) (2015) 15225–15234.
[6] T. Ouyang, K. Cheng, Y. Gao, S. Kong, K. Ye, G. Wang, et al., Molten salt synthesis of nitrogen doped porous carbon: a new preparation methodology for high-volumetric capacitance electrode materials, J. Mater. Chem. 4 (25) (2016) 9832–9843.
[7] Y. Zhang, X. Liu, S. Wang, S. Dou, L. Li, Interconnected honeycomb-like porous carbon derived from plane tree fluff for high performance supercapacitors, J. Mater. Chem. 4 (28) (2016) 10869–10877.
[8] Y. Wang, H. Dou, B. Ding, J. Wang, Z. Chang, Y. Xu, et al., Nanospace-confined synthesis of oriented porous carbon nanosheets for high-performance electrical double layer capacitors, J. Mater. Chem. 4 (43) (2016) 16879–16885.
[9] M. Oschatz, S. Boukhalfa, W. Nickel, J.P. Hofmann, C. Fischer, G. Yushin, et al., Carbide-derived carbon aerogels with tunable pore structure as versatile electrode material in high power supercapacitors, Carbon 113 (2017) 283–291.
[10] M.F. El-Kady, V. Strong, S. Dubin, R.B. Kaner, Laser scribing of high-performance and flexible graphene-based electrochemical capacitors, Science 335 (6074) (2012) 1326–1330.
[11] H. Li, Y. Tao, X. Zheng, J. Luo, F. Kang, H.-M. Cheng, et al., Ultra-thick graphene bulk supercapacitor electrodes for compact energy storage, Energy Environ. Sci. 9 (10) (2016) 3135–3142.
[12] A.G. Kannan, A. Samuthirapandian, D.-W. Kim, Electric double layer capacitors employing nitrogen and sulfur co-doped, hierarchically porous graphene electrodes with synergistically enhanced performance, J. Power Sources 337 (2017) 65–72.
[13] X.-F. Jiang, X.-B. Wang, P. Dai, X. Li, Q. Weng, X. Wang, et al., High-throughput fabrication of strutted graphene by ammonium-assisted chemical blowing for high-performance supercapacitors, Nano Energy 16 (2015) 81–90.
[14] C. Chen, D. Yu, G. Zhao, B. Du, W. Tang, L. Sun, et al., Three-dimensional scaffolding framework of porous carbon nanosheets derived from plant wastes for high-performance supercapacitors, Nano Energy 27 (2016) 377–389.
[15] X. He, H. Ma, J. Wang, Y. Xie, N. Xiao, J. Qiu, Porous carbon nanosheets from coal tar for high-performance supercapacitors, J. Power Sources 357 (2017) 41–46.
[16] J. Jin, X. Qiao, F. Zhou, Z.-S. Wu, L. Cui, H. Fan, Interconnected phosphorus and nitrogen co-doped porous exfoliated carbon nanosheets for high-rate supercapacitors, ACS Appl. Mater. Interfaces 9 (2017) 17317–17325.
[17] D. Zhu, Y. Wang, W. Lu, H. Zhang, Z. Song, D. Luo, et al., A novel synthesis of hierarchical porous carbons from interpenetrating polymer networks for high performance supercapacitor electrodes, Carbon 111 (2017) 667–674.
[18] V. Veeramani, R. Madhu, S.-M. Chen, M. Sivakumar, C.-T. Hung, N. Miyamoto, et al., NiCo2O4-decorated porous carbon nanosheets for high-performance supercapacitors, Electrochim. Acta 247 (2017) 288–295.
[19] X. Fan, C. Yu, J. Yang, Z. Ling, C. Hu, M. Zhang, et al., A layered-nanospace-confinement strategy for the synthesis of two-dimensional porous carbon nanosheets for high-rate performance supercapacitors, Adv. Energy Mater. 5

(7) (2015).
[20] K. Naoi, 'Nanohybrid capacitor': the next generation electrochemical capacitors, Fuel Cell 10 (5) (2010) 825–833.
[21] S. Ishimoto, Y. Asakawa, M. Shinya, K. Naoi, Degradation responses of activated-carbon-based EDLCs for higher voltage operation and their factors, J. Electrochem. Soc. 156 (7) (2009) A563–A571.
[22] K. Naoi, S. Ishimoto, J-i Miyamoto, W. Naoi, Second generation 'nanohybrid supercapacitor': evolution of capacitive energy storage devices, Energy Environ. Sci. 5 (11) (2012) 9363–9373.
[23] A.L. Higginbotham, D.V. Kosynkin, A. Sinitskii, Z. Sun, J.M. Tour, Lower-defect graphene oxide nanoribbons from multiwalled carbon nanotubes, ACS Nano 4 (4) (2010) 2059–2069.
[24] T. Romann, O. Oll, P. Pikma, H. Tamme, E. Lust, Surface chemistry of carbon electrodes in 1-ethyl-3-methylimidazolium tetrafluoroborate ionic liquid – an in situ infrared study, Electrochim. Acta 125 (2014) 183–190.
[25] O. Oll, T. Romann, C. Siimenson, E. Lust, Influence of chemical composition of electrode material on the differential capacitance characteristics of the ionic liquid/electrode interface, Electrochem. Commun. 82 (2017) 39–42.
[26] A. Izadi-Najafabadi, S. Yasuda, K. Kobashi, T. Yamada, D.N. Futaba, H. Hatori, et al., Extracting the full potential of single-walled carbon nanotubes as durable supercapacitor electrodes operable at 4 V with high power and energy density, Adv. Mater. 22 (35) (2010) E235–E241.
[27] L. Ye, Q. Liang, Z.-H. Huang, Y. Lei, C. Zhan, Y. Bai, et al., A supercapacitor constructed with a partially graphitized porous carbon and its performance over a wide working temperature range, J. Mater. Chem. 3 (37) (2015) 18860–18866.
[28] Y. Zhu, S. Murali, M.D. Stoller, K. Ganesh, W. Cai, P.J. Ferreira, et al., Carbon-based supercapacitors produced by activation of graphene, Science 332 (6037) (2011) 1537–1541.
[29] W. Tian, Q. Gao, Y. Tan, K. Yang, L. Zhu, C. Yang, et al., Bio-inspired beehive-like hierarchical nanoporous carbon derived from bamboo-based industrial by-product as a high performance supercapacitor electrode material, J. Mater. Chem. 3 (10) (2015) 5656–5664.
[30] D. Cazorla-Amorós, D. Lozano-Castelló, E. Morallón, M. Bleda-Martínez, A. Linares-Solano, S. Shiraishi, Measuring cycle efficiency and capacitance of chemically activated carbons in propylene carbonate, Carbon 48 (5) (2010) 1451–1456.
[31] Chang P-p, K. Matsumura, C-y Wang, T. Kinumoto, T. Tsumura, Chen M-m, et al., Frame-filling structural nanoporous carbon from amphiphilic carbonaceous mixture comprising graphite oxide, Carbon 108 (2016) 225–233.
[32] P. Chang, C. Wang, T. Kinumoto, T. Tsumura, M. Chen, M. Toyoda, Highly conductive hierarchical C/C composites to eliminate conductive agent in EDLC electrodes, ChemElectroChem 4 (11) (2017) 2793–2800.
[33] W.S. Hummers Jr., R.E. Offeman, Preparation of graphitic oxide, J. Am. Chem. Soc. 80 (6) (1958) 1339.
[34] J. Wang, M. Chen, C. Wang, J. Wang, J. Zheng, Preparation of mesoporous carbons from amphiphilic carbonaceous material for high-performance electric double-layer capacitors, J. Power Sources 196 (1) (2011) 550–558.
[35] L. Wang, J. Wang, F. Jia, C. Wang, M. Chen, Nanoporous carbon synthesised with coal tar pitch and its capacitive performance, J. Mater. Chem. 1 (33) (2013) 9498–9507.
[36] M.D. Stoller, R.S. Ruoff, Best practice methods for determining an electrode material's performance for ultracapacitors, Energy Environ. Sci. 3 (9) (2010) 1294–1301.
[37] L. Zhang, F. Zhang, X. Yang, G. Long, Y. Wu, T. Zhang, et al., Porous 3D graphene-based bulk materials with exceptional high surface area and excellent conductivity for supercapacitors, Sci. Rep. 3 (2013).
[38] S. Stankovich, D.A. Dikin, R.D. Piner, K.A. Kohlhaas, A. Kleinhammes, Y. Jia, et al., Synthesis of graphene-based nanosheets via chemical reduction of exfoliated graphite oxide, Carbon 45 (7) (2007) 1558–1565.
[39] I.K. Moon, J. Lee, R.S. Ruoff, H. Lee, Reduced graphene oxide by chemical graphitization, Nat. Commun. 1 (6) (2010) 73.
[40] A. Bagri, C. Mattevi, M. Acik, Y.J. Chabal, M. Chhowalla, V.B. Shenoy, Structural evolution during the reduction of chemically derived graphene oxide, Nat. Chem. 2 (7) (2010) 581–587.
[41] M. Sevilla, A.B. Fuertes, Direct synthesis of highly porous interconnected carbon nanosheets and their application as high-performance supercapacitors, ACS Nano 8 (5) (2014) 5069–5078.
[42] N. Jung, S. Kwon, D. Lee, D.M. Yoon, Y.M. Park, A. Benayad, et al., Synthesis of chemically bonded graphene/carbon nanotube composites and their application in large volumetric capacitance supercapacitors, Adv. Mater. 25 (47) (2013) 6854–6858.
[43] D. Puthusseri, V. Aravindan, S. Madhavi, S. Ogale, 3D micro-porous conducting carbon beehive by single step polymer carbonization for high performance supercapacitors: the magic of in situ porogen formation, Energy Environ. Sci. 7 (2) (2014) 728–735.
[44] X.-F. Hao, Y. Yan, L.-G. Gao, W.-S. Mu, C. Hao, Ionothermal synthesis of graphene-based hierarchically porous carbon for high-energy supercapacitors with ionic liquid electrolyte, Electrochim. Acta 241 (2017) 124–131.
[45] J. Hou, C. Cao, F. Idrees, X. Ma, Hierarchical porous nitrogen-doped carbon nanosheets derived from silk for ultrahigh-capacity battery anodes and supercapacitors, ACS Nano 9 (3) (2015) 2556–2564.
[46] J. Hou, K. Jiang, R. Wei, M. Tahir, X. Wu, M. Shen, et al., Popcorn-derived porous carbon flakes with an ultrahigh specific surface area for superior performance supercapacitors, ACS Appl. Mater. Interfaces 9 (36) (2017) 30626–30634.
[47] Y. Gong, D. Li, C. Luo, Q. Fu, C. Pan, Highly porous graphitic biomass carbon as advanced electrode materials for supercapacitors, Green Chem. 19 (17) (2017) 4132–4140.
[48] J. Xu, Z. Tan, W. Zeng, G. Chen, S. Wu, Y. Zhao, et al., A hierarchical carbon derived from sponge-templated activation of graphene oxide for high-performance supercapacitor electrodes, Adv. Mater. 28 (26) (2016) 5222–5228.
[49] S. Murali, N. Quarles, L.L. Zhang, J.R. Potts, Z. Tan, Y. Lu, et al., Volumetric capacitance of compressed activated microwave-expanded graphite oxide (a-MEGO) electrodes, Nano Energy 2 (5) (2013) 764–768.